From test site to flume: replication and quantification of tidal turbine blade fatigue loads in turbulent flows

Luke Myers, Tom Blackmore, Luke Blunden, and AbuBakr Bahaj

Abstract— **In this paper experiments were performed on an instrumented 1/20th scale turbine using static grids to generate turbulent flows in a circulating water flume and also at a small-scale tidal test site. Fatigue Damage Equivalent Loads (FDEL's) were calculated to allow cross comparison between different cases. The results of this research demonstrate that a wide range of turbulent flow conditions can be generated using varying geometry grids, locating the turbine at varying distances downstream. It is possible in the laboratory to closely replicate flow conditions from a real tidal site in terms of turbulence intensity and integral length scale with a corresponding replication of measured fatigue loads. There was a 5-fold increase in fatigue damage acting on the turbine at the tidal test site compared to the typical low turbulence laboratory case. It was also found that the increase in fatigue damage due to increasing turbine rotational speed was only 10% of that due to increasing ambient turbulence thus the ambient flow conditions are critical in determining fatigue loading. This work found that exact replication of turbulent characteristics was not required to match fatigue damage loads between the flume and real site, but a relatively close match was sufficient.**

Keywords— **blade loads, experiments, fatigue, test site, tidal turbine**

I. Introduction

The tidal energy industry is in the early stages of development but has the potential to provide electricity that is predictable and where peak flows between sites are offset or out of phase it has the potential to provide a degree of base load electricity generation. A number of devices have undergone pre-commercial development and testing at sites such as the European Marine Energy Centre EMEC [1]. The first commercial array developed by Meygen in the Pentland Firth, Scotland saw 4 turbines installed, commencing their operational phase early in 2018 [2]. The following phase of development (2) will see 28 MW of additional turbines to be installed by the end of 2027. Clearly there has been progress in recent years, but there are still significant challenges before the tidal energy industry is a commercial success. The key barriers are associated to cost, proving their reliability, and reducing risk for financial investment. An issue with a number of early stage devices was blade failure [3-6]. Tidal flows are highly energetic and dynamic with a broad range of characteristics including turbulence, waves, and velocity shear that differ significantly between sites [7, 8]. This is a challenging environment with high fatigue loads that could likely explain the early blade failures. The motivation of this paper is to better understand the impact of turbulence on the fatigue loads acting on a turbine blade through the accurate replication of real site flow conditions at smaller scale to help de-risk the technology and facilitate a cost-effective design process to be conducted.

Small - scale turbines have been used extensively in laboratory experiments to investigate and optimise turbine performance. These experiments are typically performed in towing tanks or large circulating flumes where steady state conditions can be achieved. The results obtained are invaluable for validation of numerical codes for predicting turbine performance [9, 10]. However, more recently there has been interest in the performance of turbines under non-uniform, non-steady state conditions due to the highly energetic conditions experienced in a tidal flow and the resulting fatigue loads. Tidal flows experience dynamic contributions from waves, turbulence generated from the seabed or other bathymetric features and from

Manuscript submitted 2 August 2022; Revised 9 September 2025; Accepted 9 September 2025. Published 20 October 2025.

Some of the work received support from MARINET, a European Community - Research Infrastructure Action under the FP7 "Capacities" Specific Programme with further support from the EPSRC grant 'Reducing the Costs of Marine Renewables via Advanced Structural Materials (ReC-ASM)'- EP/K013319/1. We also acknowledge Southern Water support for providing access to Western Jetty and allowing the development of the River Itchen tidal test site.

Luke Myers (luke@soton.ac.uk), Luke Blunden (lsb1@soton.ac.uk) and AbuBakr Bahaj (A.S.Bahaj@soton.ac.uk) are with the Energy and Climate Change Division, School of Engineering, Faculty of Engineering and Physical Sciences, University of Southampton, UK.

Digital Object Identifier: https://doi.org/10.36688/imej.8.407-416

variations in velocity shear. Whilst variability in generated power can be low with voltage variation within tolerable limits [11] it has been shown with experiments using a towing tank and wave generators that the range of blade root bending moments increased with increasing wave height. For the most extreme case tested the blade experienced a loading range of 175% the median flap-wise blade root bending moment [12]. These experiments highlighted the significant increase in blade loads when compared to the steady state case. Towing tank experiments have also been used to create a uniform oscillatory flow by superimposing an oscillatory motion to the turbine attached to the towing carriage [13, 14]. This essentially creates a simplified one-dimensional uniform unsteady flow. Flow separation was shown to result in loads significantly greater in magnitude than that for steady flow [13]. For cases where the boundary layer was believed to be attached to the outer sections of the blade, the out-of-plane bending moment amplitude for unsteady flow was up to 15% greater than the corresponding load measured in steady flow and exhibited a phase-lead of up to 4.5 degrees. Both these observations were believed to be qualitatively consistent with the effects of dynamic inflow and non-circulatory forcing [14]. Experimental work has shown that blade root streamwise load variations increase in progressively sheared velocity profiles [15] as one might expect.

Flume experiments have also been used to investigate the effects of turbulence upon turbine thrust and power by generating additional turbulence in the facility. Early studies considered the effects of turbulence intensity which is the ratio of Root Mean Square (R.M.S) velocity fluctuations to the mean velocity and typically expressed as a percentage. The results showed a reduction in turbine thrust and power coefficients of approximately 10% when the turbulence intensity increased from 8% to 25% [16]. However, little information was presented on the structure of turbulence. Small scale experiments using porous disc rotor simulators showed that the turbulence length scales were also an important parameter to consider, typically the integral length scale is used which can be thought of as the size of eddies containing the greatest proportion of turbulent energy in the flow. It was shown that flows with different integral length scales resulted in variations in thrust coefficient of over 20% [17]. These experiments used static grids to generate turbulent flows in the flume with different intensities and length scales. The use of static grid turbulence generation is well understood for wind tunnel experiments and produces approximately uniform isotropic turbulence [18]. Turbulent eddies are generated downstream of the grid bars, their size proportional to the bar width. The turbulence in the flow dissipates with distance downstream from the grid and may be described by a turbulence decay power law [19]. Therefore the turbulence length scale may be controlled by changing the size of the grid bars, and the turbulence intensity may be controlled with the position downstream from the grid. Experiments have use static grid turbulence generators in a circulating water flume with a $1/20^{th}$ scale turbine installed in the turbulent flow [20]. The results show that the turbine performance (power and thrust coefficients) is sensitive to the turbulence characteristics of the flow. It was postulated that turbulence length scales of the order of turbine diameter interact strongly with the wake resulting in an increased flowrate through the turbine and increase the mean loads acting on the rotor. Length scales less than a quarter of the rotor diameter interact directly with the blade and tend to reduce performance with increasing turbulence intensity. The same trends were found on a second turbine subjected to the same turbulent conditions [21]. These previous studies focus on the impact of turbulence on the mean performance of the turbine and show how the rotor loads and blade root bending moments are directly linked. However, it can also be seen that increasing the turbulence length scale or turbulence intensity increases the magnitude, and frequency of load fluctuations [17, 22, 23]. This will have a significant impact on the fatigue life of the turbine. Furthermore it has been shown that rotor control strategy of constant torque or rotor speed will have differing effects upon rotor power [24].

Fatigue is intrinsically linked to the materials under load, in this case the blades. Research has been conducted using accelerated aging of composites to replicate tidal turbine blades towards the end of their operational life [25]. Seawater immersion was shown to increase the amount of water absorbed by the composite material with a corresponding decrease in fatigue life for typical operating conditions. Increasing laminate thickness could counteract the effects of water absorption and weakening of the blade material albeit at additional cost. Other work [26] used material testing results to design and simulate loading cases on tidal turbine blades. Important outputs showed that glass fibre was inadequate as a material and a hybrid glass and carbon fibre material was required. A device failure scenario was simulated whereby the blade pitch mechanism failed at the rated flow speed and power and torque produced was 100% above rated values. In these cases the design loads were exceeded. In a practical case this could lead to either blade failure or the need for inspection both of which have significant cost implications. Whilst operational costs are not yet fully understood and may vary between device types at the early stages of the technology there have been estimates of operational costs with unplanned maintenance accounting for a little under 30% for devices in an array [27]. The corresponding value for planned maintenance is also 30% thus any knowledge and understanding that can inform device design and control to minimise any interventions will drive down operational costs.

Fatigue and reliability analyses have previously been conducted for wind turbines using probabilistic modelling [28]. Further studies have been undertaken in the wind industry using large experimental datasets of turbine

loads recorded over a number of months [29]. In such work the results were normalised to present an equivalent fatigue load of constant amplitude, this allowed different datasets to be directly compared. These datasets were important for the development of numerical models to predict reliability and fatigue life of wind turbines. Further numerical studies have used probabilistic models to assess the reliability of tidal turbine blades which could be used at the design stage [30]. More recently a CFD model has been used to output time-series data of the blade loads acting on a tidal turbine in a turbulent flow [31]. In this study a Fatigue Damage Equivalent Load (FDEL) was used to allow direct comparison of results with different levels of ambient turbulence. The FDEL is a constant amplitude load cycle that would result in equivalent fatigue damage, thus allowing comparison between different cases. This method has been used in the wind industry to investigate the fatigue damage on both turbine rotors and mono-piles for offshore turbines [29], [32]. The report further emphasises the need for high resolution site data of tidal flows that can capture the full spectrum of turbulent scales as it was found that turbine performance is sensitive to both length scale and intensity of turbulence. In mid-large scale turbulence an increase in power output was observed indicating conservative estimates from towing tank experiments or Blade Element Momentum models, this is consistent with previous experimental results [20]. To this end there has been some work to couple measured tidal site flow data with computer models of a turbine [33]. This particular study used a Blade Element Momentum code which is prevalent in the nascent stages of the tidal energy industry due to its computational efficiency. Differences in FDEL of circa 30% were found between both changing the rotor hub height and also the local spatial location of a device indicating the variability in load cases. The coupling of measured site data to Reynolds-Averaged Navier-Stokes (RANS) has also been conducted [34] to investigate the influence of both supporting structures and vertical velocity profiles on blade loading again with loads varying by as much as 43% of the maximum total thrust force. High-fidelity models such as Large Eddy Simulation (LES) are now more prevalent given advances in computational resources. They have been used to investigate blade root loadings of devices simulated in various array configurations of multiple devices [35].

It is also worth noting that experimental turbulence measurements are typically made from point measurements of velocity due to experimental practicalities. However, due to the rotational speed of the turbine, the rotor the blades will be subjected to a modified spectrum of turbulence due to their rotation. The effects of rotationally sampled turbulence have been investigated for wind turbines and found to have an effect for low frequency fluctuations. However, above twice the rotational frequency it was found that any fluctuation is almost entirely due to turbulence [36].

In this work we use a fully instrumented 0.8 m-diameter (≈1/20th scale) tidal turbine to investigate the blade root fatigue loads when the turbine was operated in different real flow conditions. Experiments have been performed in a large circulating water flume with different levels of turbulence, generated using static grids [20]. Measurements were made across a range of turbine rotational speeds to assess the relative importance of rotational effects in comparison to turbulence. The results from these laboratory experiments are also compared to a series of experiments performed at a small scale tidal test site in the river Itchen, Southampton, UK [37]. Flow characteristics were quantified using standard offshore diverging beam instruments (ADCP) but importantly it was possible at the site to use high frequency converging beam laboratory instruments to determine higher-order flow properties such as turbulent length scale. A rain flow algorithm is used to count the fatigue cycles and a Fatigue Damage Equivalent Load (FDEL) used for direct comparisons between tests. While these results are from small scale experiments, the results provide a key dataset of turbine blade loads when operating in different conditions, and more importantly a direct comparison of the laboratory results to a small-scale deployment in a tidal estuary providing a different approach of [33,34] where real flow data is used in simulations.

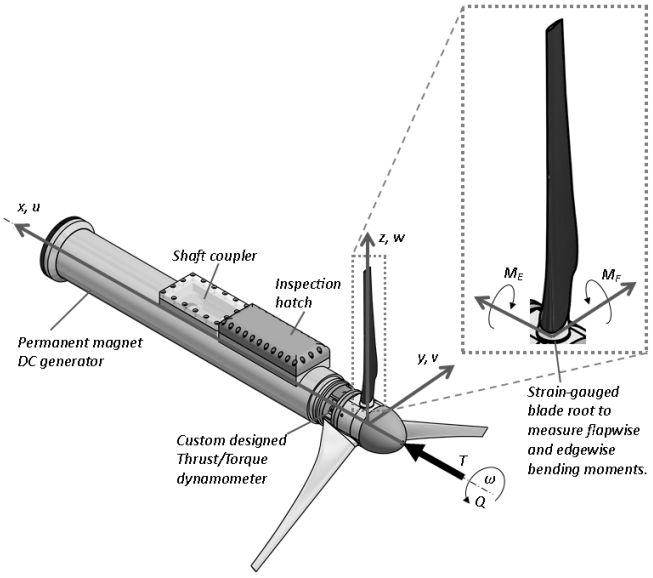

Fig. 1. Turbine details and coordinate system.

II. Experimental Method

A. Turbine

The turbine used in this work is a 1/20th scale, 0.8 m diameter three-blade horizontal axis tidal turbine developed by the University of Southampton. Further design details can be found in [12, 20]. The diameter is variable and the 0.8 m diameter rotor was chosen for operation in larger indoor test facilities. Figure.1 shows a diagram of the turbine and the coordinate system used herein. The turbine uses a custom-designed thrust/torque dynamometer located immediately behind the rotor hub

and upstream of all seals, bearings and the power take-off subsystem thus quantifying the true rotor loads. One of the turbine blades was fitted with strain gauges on the blade root to measure the flapwise and edgewise blade root bending moments. The blades use a NACA 48XX profile with varying thickness and twist along the blade length. A hollow shaft encoder was used to provide accurate rotor velocity and azimuthal position of the gauged blade. Data and electrical power in/out was conveyed to/from the surface via a flexible umbilical cable exiting the rear of the nacelle. Turbine data was acquired at 200 Hz with the turbine rotor speed controlled using a feedback loop connected to a fast response electronic load to maintain constant rotational speed. The total uncertainty in blade load measurements was less than 1.5% of the mean blade root bending moment [20]. A minimum sample time of 300s was used resulting in a sampling error of less than 1%, as described in [20].

The turbine was operated at close to peak power coefficient at a Tip-Speed-Ratio (TSR) of approx. 5.5. TSR is defined as the ratio between the blade tip speed and the free-stream flow speed. Key rotor performance characteristics include the power captured and the thrust force acting upon the rotor. Both can be expressed non-dimensionally:

$$C_p = \frac{P}{0.5\rho U^3 A} \tag{1}$$

$$C_t = \frac{T}{0.5\rho U^2 A} \tag{2}$$

Where C_P is the power coefficient, P is the generated power (Watts), ϱ is the fluid density (kg.m^{-3}) U is the freestream velocity (m.s^{-1}), A is the rotor area (m^2), T is the rotor thrust (Newtons) and C_t is the thrust coefficient.

The typical measured non-dimensionless thrust-power curves for the turbine are shown in Figure 2.

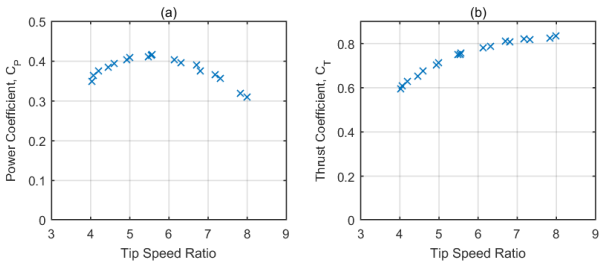

Fig.2. Turbine power and thrust coefficients at varying tip speed ratio.

The blade set has been used extensively in previously published works over a range of flow speeds encompassed within this paper. For steady flows indicates power and thrust coefficient behavior consistent with larger devices indicating Reynolds independence [38].

B. *Circulating flume experiments*

Laboratory experiments were performed in the IFREMER circulating water channel in Boulogne-Sur-Mer, France which is 4 m wide, 2 m deep, and a working section 18 m in length [39]. The flow velocity and turbulence characteristics were quantified using a Dantec 2D Laser Doppler Velocimeter (LDV) with typical sampling frequency of 350 Hz. There is a degree of ambient turbulence in the channel and additional turbulence was generated using two static grids of different geometry detailed in [20]. The grids generate approximately uniform, isotropic turbulence to within 10% in the streamwise and transverse directions [20] as expected from theory [19]. The downstream location of the turbine from the grid was varied to generate flows with different turbulence intensities and turbulence length scales.

The turbine was operated in the different turbulent flows as shown in Figure 3 and its performance recorded.

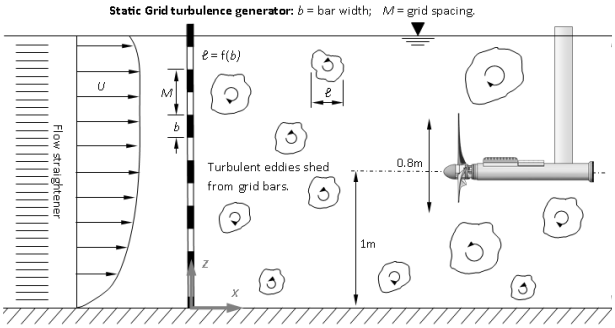

Fig. 3. Schematic of laboratory experiments adapted from [20].

It was shown that increasing turbulence intensity tended to reduce the power generated by the turbine. However, it was found that increasing the turbulence length scales tended to increase power [20]. More significantly the load fluctuations also increased with increasing turbulence, and this is the focus of this paper.

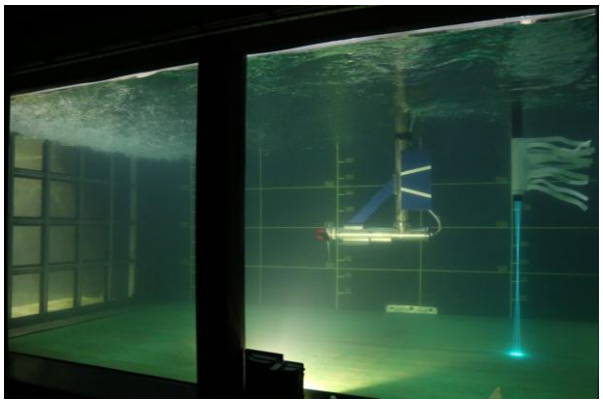

Fig. 4. turbine installed and operating downstream of turbulence grid with the Laser Doppler Velocimeter quantifying flow downstream of the turbine.

C. *River Itchen experiments*

A small-scale tidal turbine test site has been developed in the River Itchen, Southampton UK, by the University of Southampton and access to the site provided by Southern Water. Figure 5 shows the location of the test site which is attached to the end of Weston Jetty Pier and aligned with the ebb flow of the river Itchen. The rise and fall of tide is approximately 5 m on a spring tide and the maximum water depth at the site at spring tides is approximately 5.5 m with a level bed in the proximity of the turbine.

Fig. 5. Location of River Itchen tidal turbine test site in Southampton, UK (left) and aerial view (right).

Characterisation of the flow has been previously reported following deployment of a Nortek Acoustic Doppler Current Profiler (ADCP) and converging beam Nortek Vectrino + Acoustic Doppler Velocimeter (ADV) [37]. The site has a maximum ebb flow during spring tides of approximately 0.6 m/s which lasts a duration of approximately 30 minutes for operating the turbine with negligible variation in flow direction allowing the turbine rotor to be aligned perpendicular to the flow. The ebb tide is stronger due to velocity component added by the river. For the reporting herein the average velocity across the rotor was 0.52 m/s, the turbulence intensity was measured at 20.7% with integral length scales of 0.14 m.

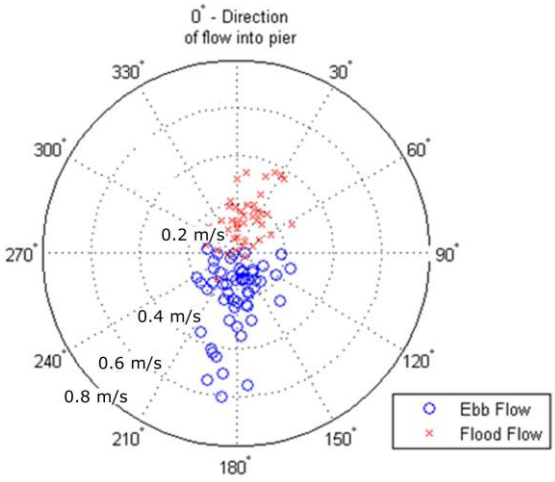

Fig. 6. Velocity distribution at 1.78m from sea bed. Data from Flood and Ebb flows during a spring tide

From Figure 6 it can be seen that lower velocities occur during the flood tide. There is always a discharge flow from the river into the estuary in the same direction as the ebb flow and opposing the flood flow. Also, the presence of the pier legs obstructs the flood flow leaving the measurement location in a slow-moving wake. During the faster moving flood tide flows (above 0.4 m/s), the flow angles vary by up to 30 degrees. The slower moving flows show much more variability in direction.

The turbine was attached to a sliding support frame and could be lowered into the water using a crane/winch to a depth of approximately 1 m below the surface, to be consistent with the submersion depth of the laboratory experiments while capturing the maximum flow speed. Figure. 7 shows the turbine frame attached to the pier via the winch system. Two Nortek Vectrino + ADVs were used to record the flow speed at the top right, and bottom left (viewed from the pier) beyond the rotor's swept frontal area.

D. *Summary of experimental flow conditions*

Table 1 shows a summary of the flow conditions for the four cases in which the turbine was operated. These cases provide the comparisons presented in this work. Due to the variations in velocity for the different cases, 0.5 - 0.8 m/s, loads will be normalised using the mean velocity in each case.

TABLE I
SUMMARY OF FLOW CONDITIONS FOR FOUR TEST CASES

		Velocity (m/s)	Intensity (%)	Integral length scale (m)
Lab	No grid	0.81	4.5	0.74
	Small grid	0.76	14.8	0.18
	Large grid	0.72	17.8	0.38
Test Site		0.52	20.7	0.14

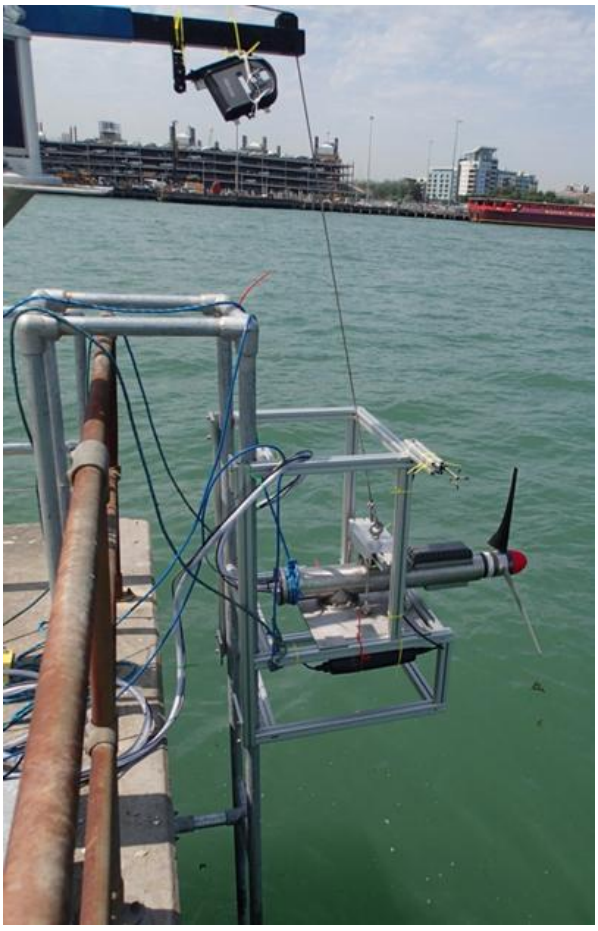

Fig. 7. River Itchen tidal turbine test site deployment.

One further experiment was performed in the flume with no grid installed and a flow speed of 0.5 m/s. This was to allow direct comparison to the site experiments where the typical tidal flow speed across the turbine was ~0.5 m/s.

III. FATIGUE CALCULATIONS

Both flapwise and edgewise blade root bending moments were recorded in the experiments (as defined in Figure 1) and the resultant blade root bending moment calculated as follows.

$$M_B = \sqrt{M_F^2 + M_E^2} \tag{3}$$

Where subscripts F and E refer to flapwise and edgewise moments respectively, B refers to the resultant. Due to the difference in flow speed of 0.5 m/s at the river Itchen tidal test site and ~0.8 m/s in the laboratory experiments, bending moments have been normalised by the square of the mean velocity such that comparisons between the normalised fluctuations can be made.

An energy spectra of the blade root bending moment was calculated using the following equations:

$$S(\omega) = \frac{2}{\pi}\int_0^\infty R(s)\cos(\omega s)\,ds \tag{4}$$

$$R(s) = \langle M_B{}'(t) M_B{}'(t+s) \rangle \tag{5}$$

Where S(ω) is the power spectral density in wavenumber space, R(s) is the autocovariance function, ω is the angular speed (Rad/s), s is the time lag, t it time. The angled brackets represent time-averaging and MB′ is the root bending fluctuation to respect to time (t) and time plus lag (t + s).

A Rainflow Counting algorithm was used to count the number of blade root bending moment cycles, the amplitude, and the range of those cycles. A MATLAB rainflow counting toolbox was used, further details can be found on the implementation of the method [40]. This method assumes that the loading cycles, at each amplitude, can be considered independent, and the order in which they are applied does not matter. Once the loading cycles of the variable amplitude time signal have been counted, a Fatigue Damage Equivalent Load (FDEL) can be calculated to allow direct comparison of the fatigue loads applied under each test case. The FDEL represents the fatigue damage accrued from a variable amplitude loading cycle, as counted using the rainflow algorithm, as a single amplitude load cycle over a given period.

$$FDEL = \left[\frac{\sum \Delta M_{Bi}{}^m n_i}{N}\right]^{1/m} \tag{6}$$

Where m is the slope of S-N fatigue curve and assumed m=8, representing a conservative value for a composite material [41], n_i is the number of cycles at amplitude M_{Bi} and N is time sample length.

IV. RESULTS AND DISCUSSION

A. Raw data

A 30-second sample of normalised raw data is shown in Figure 8 for the resultant blade root bending moment. It can be seen qualitatively that the magnitude of fluctuations increases with increasing turbulence in the laboratory experiments. Figure 8 (d) shows the raw data for the River Itchen test site and it can be seen that the fluctuations are comparable to the highest turbulence laboratory case (c) in magnitude, but the frequency appears lower compared to the laboratory cases. The lower frequency of fluctuations for the river Itchen test site could be due to the lower velocity and hence lower rotational speed of the turbine to maintain a fixed TSR.

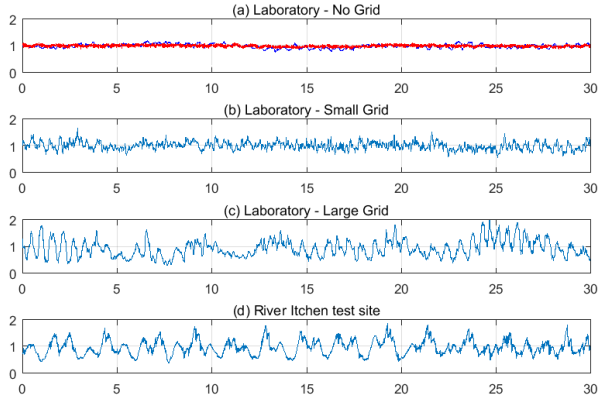

Fig. 8. Normalised blade root bending moment raw data for laboratory cases (a) no grid (red line U=0.5m/s, blue line U-0.8m/s), (b) small grid (c) large grid and (d) for River Itchen test site.

B. Histograms of loads

Figure 9 shows box plots for the normalised blade root bending moment. It can be seen that the range of loads increases with increasing turbulence from approx. 1±0.25 for the no grid case to approx. 1±1 for the test site. The median is also slightly less than 1 for the large grid and test site cases, suggesting skewness in the loads. It can also be seen that the interquartile range is comparable for the large grid and test site cases, but the test site has slightly larger extreme values.

Normalised histograms have been plotted for the flow velocity and blade root bending moments in Figure 10. It can be seen in Figure. 10 (b) that for the low turbulence case in the laboratory, the blade root bending moments are within a tight range of $0.75<M_B<1.25$ for both U=0,5 m/s and U=0.8 m/s. Increasing the turbulence using the small grid to I=14.8% and ℓ=0.18 m and large grid to I=17.4% and ℓ=0.38 m resulted in the range of loads increasing to $0.5<M_B<1.5$, and $0.25<M_B<2.25$ respectively. It is interesting to note that the histogram for the high turbulence

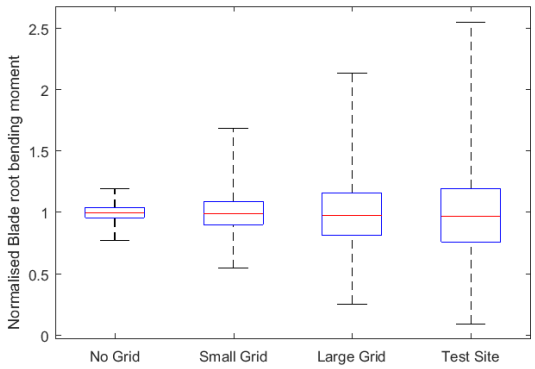

Fig. 9. Box plots for maximum to minimum range for (a) normalised blade root bending moment.

laboratory case is very close to the River Itchen test site experiment (red line). In these two cases the histogram appears skewed with a tail extending to higher loads. The shape of histogram for blade root bending moment was comparable between the laboratory case with large grid installed and the tidal test site. This suggests that the method of using static grids to create turbulence could be used to create similar levels of fatigue compared to those experienced at a tidal site.

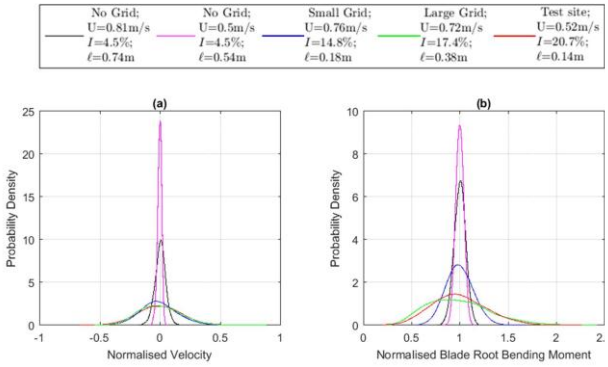

Fig. 10. Histogram of (a) normalised velocity and (b) blade root bending moment.

C. *Power spectral density*

Figure 11 shows the power spectral density of the velocity and blade root bending moment. Oblique lines indicate the -5/3 gradient. It can be seen in Figure. 11(a) that the low turbulence laboratory case contains the lowest energy across all frequencies. Increasing the velocity from U=0.5 m/s to U=0.8 m/s shows an increase in turbulence across all frequencies. A dip in the spectra is visible for these 2 cases for frequencies around 10 Hz, the cause of this was due to noise created by the pumps which was not visible with the grids installed. This was discussed further in [20]. It can also be seen in the test site measurements that there is a spike at around 0.5 Hz, this corresponds to waves observed during the measurements. It can be seen in Figure. 11(b) for the blade root bending moment spectra that there is a spike at around 1.3 Hz which corresponds to the rotational speed of the turbine. For U=0.5 m/s this spike is visible at around 0.7 Hz. Further modes can be seen at ~2.6 Hz and ~4 Hz. While the spectra of the small and large grids are comparable for frequencies greater than 3 Hz, the large grid results in higher energy at lower frequencies.

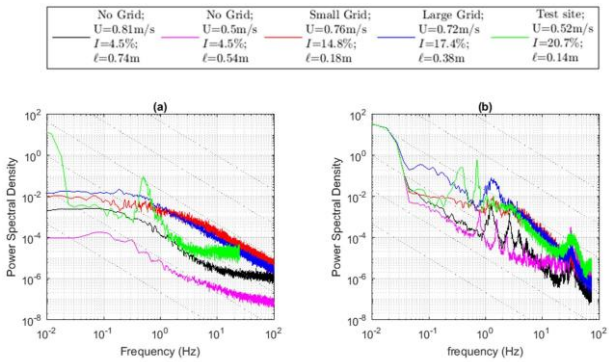

Fig. 11 Power spectral density of (a) velocity and (b) blade root bending moment. (Oblique lines indicate the -5/3 gradient)

This is to be expected due to the larger turbulence length scales for the large grid compared to the small grid. When the grids are installed the peaks in the spectra relating to the rotational speed of the turbine are less pronounced. The spectra of the river Itchen test site experiments shows similar trends to the laboratory case with the grids installed. However, there are two very dominant peaks at ~0.4 Hz and ~0.7 Hz. The 0.7 Hz peak corresponds to the rotational speed of the turbine, whereas the 0.4 Hz peak was due to the waves observed on the day the measurements were taken. Note the peak at ~0.4 Hz seen in the blade spectra is lower than seen in the velocity spectra due to the rotation of the turbine blades. The blade root bending spectra for the higher turbulence cases demonstrate a steeper power law behavior in the inertial frequency sub-range consistent with previous studies [42,43].

D. *Fatigue analysis*

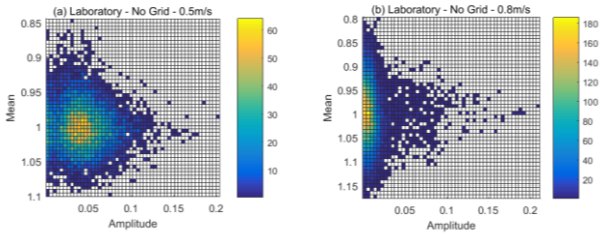

Fig. 12. Rainflow fatigue cycle count of normalised blade root bending moments for laboratory experiments with no grid and (a) 0.5m/s and (b) 0.8m/s flow speed.

Figure 12 shows the mean, amplitude, and number of stress cycles for the normalised blade root bending moment with no grid installed in the flume for (a) U=0.5 m/s and (b) U=0.8 m/s flow speeds. It can be seen that the mean and amplitudes of fluctuation are comparable between both cases ranging from 0.8<mean<1.2, and 0<amplitude<0.2. However, it can be seen that the loading cycles are more focused for the U=0.8 m/s case with a mean of ~1 and amplitude<0.05. The load cycles are more spread out for the U=0.5 m/s case with amplitudes generally less than 0.1. The FDEL was calculated to be 0.126 for U=0.5 m/s

and 0.121 at U =0.8 m/s showing little variation in the equivalent fatigue load across a range of flow speeds from U=0.5 m/s to U=0.8 m/s. This is consistent with previous results that showed the standard deviation of rotor thrust was insensitive to flow speed [44].

Figure 13 shows the rainflow counts for the normalised blade root bending moments for (a) no grid installed in flume, (b) small grid installed in flume, (c) large grid installed in flume, and (d) River Itchen tidal test site. It can be seen that the shape of each plot is similar, although the large grid and river Itchen test site show some skewness with a tail extending to a mean of over 2. As the turbulence is increased in the flume from cases a-c, it can be seen that the number of cycles and the range of mean cycles and their amplitudes increases. They increase from 0.8<mean<1.2, amplitude <0.2, and count<150 for the no grid case up to 0.4<mean<2, amplitude<0.9, and count<300 for the large grid.

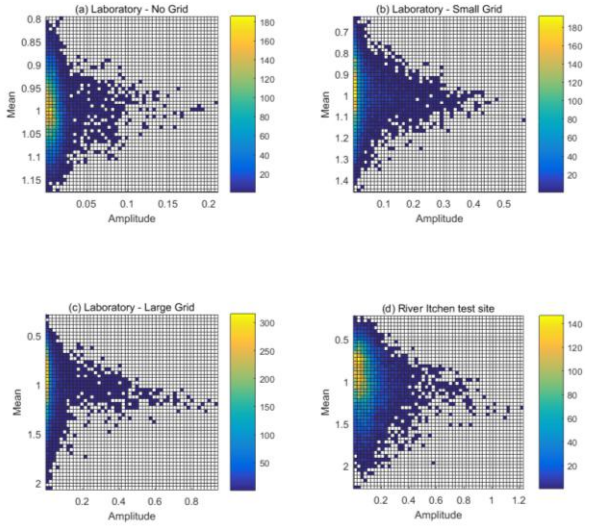

Fig. 13 Rainflow fatigue cycle count of normalised blade root bending moments for laboratory and Itchen river test site cases.

Figure 14 shows the FDEL for the normalised blade root bending moment. Increasing the turbulence in the flume shows an increase in FDEL from ~0.12 with no grid installed, to FDEL~0.33 for the small grid and FDEL~0.56 for the large grid. The FDEL for the river Itchen test site is ~0.60 which is only slightly larger than the large grid in the flume but corresponds to a 5-fold increase in fatigue damage over the typical low turbulence flume case. This highlights the need to match turbulent flow characteristics as done in this work to obtain representative fatigue damage loads. These observed results are also in agreement with previous numerical simulations that showed a 5-fold increase in FDEL when turbulence intensity was increased from 0% to 16% [31].

During the laboratory campaign the turbine was operated over a range of tip-speed-ratios (TSR). The normalised fatigue damage equivalent loads were calculated over the range 4<TSR<8. It can be seen in Figure 15 that for all cases there is a linear increase in FDEL with

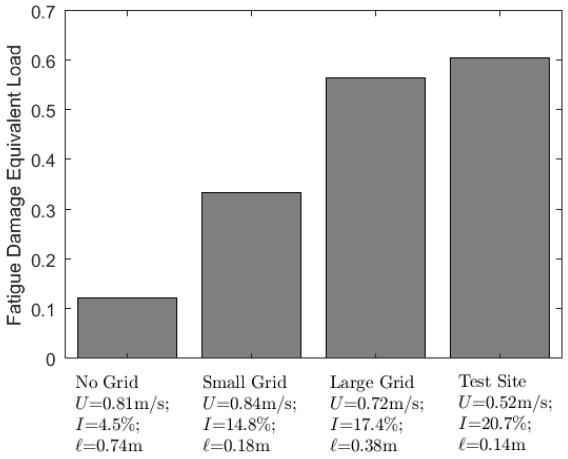

Fig. 14 Fatigue Damage Equivalent load for the normalised blade root bending moment.

increasing TSR. The increase in FDEL across all cases is approximately 0.05-0.1 from TSR=4 to TSR=8, and due to the increased rotational speed of the turbine. However, compared to the overall range in FDEL from 0.1 in low turbulence conditions to over 0.9 in the highest turbulence conditions the effect of turbine rotational speed is approximately 10% of the increase due to free stream turbulence which has a much more pronounced effect.

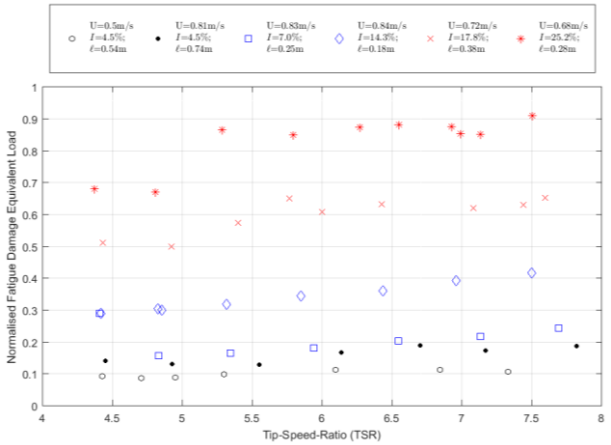

Fig. 15 Fatigue Damage Equivalent Load (FDEL) for normalised blade root bending moment at different Tip Speed Ratios (TSR).

V. CONCLUSIONS

Experiments have been performed on a 1/20th scale 0.8 m diameter horizontal axis three bladed tidal turbine to investigate the effects of turbulence on the fatigue loads acting on the turbine blade root. The key findings of this work are:

Increasing turbulence intensity and length scale increases the frequency and magnitude of load fluctuations.

A 5-fold increase in the fatigue damage on the blade root bending moment was found for the tidal test site compared to the typical low turbulence laboratory conditions.

The use of static grid turbulence generators to produce high levels of turbulence in the laboratory flume resulted in comparable fatigue damage to the tidal test site. This suggests this method is appropriate for turbine optimisation in high turbulence flows, as found at tidal sites.

Increasing the turbine rotational speed resulted in an increase in fatigue damage. However, the increase in fatigue damage due to turbine rotational speed was only 10% of the increase due to increasing ambient turbulence.

The key impact of this work is two-fold: firstly demonstrating the increase in fatigue loads with increased turbulence. By understanding the impact of turbulence on the relative increase in fatigue loads the turbine blades can be optimised for reliability while minimising cost. Secondly the experimental method using static grid turbulence generators succeeded in producing comparable levels of fatigue damage to the small-scale test site through accurate flow characterisation and replication. This method should therefore be used for laboratory scale R&D turbine testing in favour of the typical low turbulence laboratory conditions. It does however require good quality site measurements and reasonable time at the controlled laboratory facility in order to characterise the turbulent properties of the flow downstream of any grid-type structure.

These findings highlight how significant the fatigue loads are when operating in a highly turbulent tidal flow. If turbines are designed using typical low turbulence conditions, fatigue loads will be severely underestimated resulting in poor reliability. For laboratory scale experiments the use of static grid turbulence generators can be used to produce comparable levels of fatigue damage to a real tidal flow. If turbines are designed for these site-specific highly turbulent flows, reliability can be optimised, reducing risk and operating costs helping the industry move closer to commercialisation.

REFERENCES

[1] EMEC, "European Marine Energy Centre," [Online]. Available: https://www.emec.org.uk/projects/ [Accessed: 11-Sept-2025].

[2] MEYGEN, project details [Online] Available: https://en.wikipedia.org/wiki/MeyGen. [Accessed: 11-Sept-2025]

[3] BBC, "Blade fault on giant tide turbine AK1000 in Orkney," BBC, 2010. [Online]. Available: http://www.bbc.co.uk/news/uk-scotland-highlands-islands-11492829. [Accessed: 11-Sept-25].

[4] Researchgate – image of Verdant power turbine [Online]. Available: https://www.researchgate.net/figure/Blade-of-Verdant-Powers-tidal-turbines-that-failed_fig1_378247063. [Accessed: 11-Sept-25].

[5] Control subsystem fault leads to damage of SeaGen's rotors [Online]. Available: https://en.wikipedia.org/wiki/Marine_Current_Turbines. [Accessed: 11-Sept-25].

[6] R. Shulman, "N.Y. Tests Turbines to Produce Power," The Washington Post, 2008. [Online]. Available: http://www.washingtonpost.com/wp-dyn/content/article/2008/09/19/AR2008091903729.html. [Accessed: 11-Dec-2025].

[7] I. A. Milne, R. N. Sharma, R. G. J. Flay, and S. Bickerton, "Characteristics of the turbulence in the flow at a tidal stream power site," Phil Trans R Soc A, vol. 371, no. 1985, pp. 1–14, 2013.

[8] J. Thomson, B. Polagye, V. Durgesh, and M. C. Richmond, "Measurements of Turbulence at Two Tidal Energy Sites in Puget Sound, WA," IEEE J. Ocean. Eng., vol. 37, no. 3, pp. 363–374, Jul. 2012.

[9] A. S. Bahaj, W. M. J. Batten, and G. McCann, "Experimental verifications of numerical predictions for the hydrodynamic performance of horizontal axis marine current turbines," Renew. Energy, vol. 32, no. 15, pp. 2479–2490, Dec. 2007.

[10] W. M. J. Batten, A. S. Bahaj, A. Molland, and J. Chaplin, "The prediction of the hydrodynamic performance of marine current turbines," Renew. Energy, vol. 33, no. 5, pp. 1085–1096, May 2008.

[11] Lewis, M., McNaughton, J., Márquez-Dominguez, C., Todeschini, G., Togneri, M., Masters, I., Allmark, M., Stallard, T., Neill, S., Goward-Brown, A. and Robins, P., 2019. Power variability of tidal-stream energy and implications for electricity supply. *Energy*, *183*, pp.1061-1074.

[12] P. W. Galloway, L. E. Myers, and A. S. Bahaj, "Quantifying wave and yaw effects on a scale tidal stream turbine," Renew. Energy, vol. 63, pp. 297–307, Mar. 2014.

[13] I. A. Milne, A. H. Day, R. N. Sharma, and R. G. J. Flay, "Blade loads on tidal turbines in planar oscillatory flow," Ocean Eng., vol. 60, pp. 163–174, 2013.

[14] I. A. Milne, A. H. Day, R. N. Sharma, and R. G. J. Flay, "Blade loading on tidal turbines for uniform unsteady flow," Renew. Energy, vol. 77, pp. 338–350, 2015.

[15] Magnier, M., Delette, N., Druault, P., Gaurier, B. and Germain, G., 2022. Experimental study of the shear flow effect on tidal turbine blade loading variation. *Renewable Energy*.

[16] F. Maganga, G. Germain, J. King, G. Pinon, and E. Rivoalen, "Experimental characterisation of flow effects on marine current turbine behaviour and on its wake properties," IET Renew. Power Gener., vol. 4, no. 6, p. 498, 2010.

[17] T. Blackmore, W. M. J. Batten, G. U. Muller, and A. S. Bahaj, "Influence of turbulence on the drag of solid discs and turbine simulators in a water current," Exp. Fluids, vol. 55, no. 1, p. 1637, Dec. 2014.

[18] P. E. Roach, "The generation of nearly isotropic turbulence by means of grids," Heat fluid flow, vol. 8, no. 2, pp. 82–92, 1987./

[19] S. B. Pope, Turbulent Flows. Cambridge University Press, 2000.

[20] T. Blackmore, L. E. Myers, and A. S. Bahaj, "Effects of Turbulence on Tidal Turbines: Implications to Performance, Blade loads, and Condition Monitoring," Int. J. Mar. energy, vol. 470, no. 2170, pp. 1–26, 2016.

[21] T. Blackmore, B. Gaurier, L. E. Myers, G. Germain, and A. S. Bahaj, "Turbulence and tidal turbines," in 11th European Wave and Tidal Energy Conference, 2015.

[22] A. S. Bahaj and T. Blackmore, "Design guidance on device layout within arrays," Int. J. Mar. Energy, 2016.

[23] T. Blackmore, W. M. J. Batten, and A. S. Bahaj, "Influence of turbulence on the wake of a marine current turbine simulator," Proc. R. Soc. A, vol. 470, 2014.

[24] Allmark, M., Ellis, R., Ebdon, T., Lloyd, C., Ordonez-Sanchez, S., Martinez, R., Mason-Jones, A., Johnstone, C. and O'Doherty, T., 2021. A detailed study of tidal turbine power production and dynamic loading under grid generated turbulence and turbine wake operation. *Renewable Energy*, *169*, pp.1422-1439.

[25] C. Kennedy, V. Jaksic, S. Leena and C. Brádaigh, "Fatigue life of pitch- and stall-regulated composite tidal turbine blades," Renew. Energy, vol. 121, pp. 688–699, 2018.

[26] E. M.Fagan, C. R. Kennedy, S.B. Leen and J. Goggins, "Damage mechanics based design methodology for tidal current turbine composite blades", Renew. Energy, vol. 97, pp. 358–372, 2016.
[27] Carbon Trust - marine energy technical reports [Online] Available: https://www.carbontrust.com/media/173551/capital-operating-and-maintenance-costs.pdf. [Accessed: 11-Apr-19]
[28] K. O. Ronold, J. Wedel-Heinen, and C. J. Christensen, "Reliability-based fatigue design of wind-turbine rotor blades," Eng. Struct., vol. 21, no. 12, pp. 1101–1114, 1999.
[29] P. Ragan and L. Manuel, "Comparing Estimates of Wind Turbine Fatigue Loads using Time-Domain and Spectral Methods," Wind Eng., vol. 31, no. 2, pp. 83–99, 2009.
[30] D. V. Val, L. Chernin, and D. V. Yurchenko, "Reliability analysis of rotor blades of tidal stream turbines," Reliab. Eng. Syst. Saf., vol. 121, pp. 26–33, 2014.
[31] T. Clark, T. Roc, S. Fisher, and N. Minns, "Turbulence and turbulent effects in turbine and array engineering: A guide for the tidal power industry," Doc: MRCF-TiME-KS10. OAS & IT Power, 2015.
[32] E. Marino, A. Giusti, and L. Manuel, "Offshore wind turbine fatigue loads: The influence of alternative wave modelling for different turbulent and mean winds," Renew. Energy, vol. 102, pp. 157–169, 2017.
[33] H. Mullings, T. Stallard, "Assessment of Dependency of Unsteady Onset Flow and Resultant Tidal Turbine Fatigue Loads on Measurement Position at a Tidal Site" Energies, 14, 5470, 2021.
[34] W.Finnegan, E. Fagan, T. Flanagan, A.Doyle, J. Goggins "Operational fatigue loading on tidal turbine blades using computational fluid dynamics" Renewable Energy, V. 152, 2020.
[35] P. Ouro, L. Ramírez, M. Harrold, "Analysis of array spacing on tidal stream turbine farm performance using Large-Eddy Simulation" journal of fluids and structures vol. 91, 2019
[36] R. L. George and J. R. Connell, "Rotationally sampled wind characteristics and correlations with MOD-0A wind turbine response." 1984.
[37] K. Shah, T. Blackmore, L. Blunden, L. E. Myers, and A. S. Bahaj, "From lab to field: deployment of a scale turbine in a tidal estuary," in EWTEC, 6-11th Sept, Nantes, France, 2015.
[38] Pascal W. Galloway, Luke E. Myers, AbuBakr S. Bahaj "Experimental and numerical results of rotor power and thrust of a tidal turbine operating at yaw and in waves" World Renewable Energy Congress, Linkoping, Sweden, 2011.
[39] G. Germain, A. S. Bahaj, C. Huxley-Reynard, and P. Roberts, "Facilities for marine current energy converter characterisation," in 7th European Wave and Tidal Energy Conference, 2007.
[40] A. Niesłony, "Determination of fragments of multiaxial service loading strongly influencing the fatigue of machine components," Mech. Syst. Signal Process., vol. 23, no. 8, pp. 2712–2721, 2009.
[41] G. Freebury and W. Musial, "Determining equivalent damage loading for full-scale wind turbine blade fatigue tests," 2000 ASME Wind Energy Symp., no. February, p. 12, 2000.
[42] Deskos, G., Payne, G.S., Gaurier, B. and Graham, M., 2020. On the spectral behaviour of the turbulence-driven power fluctuations of horizontal-axis turbines. *Journal of Fluid Mechanics*, *904*.
[43] Allmark, M., Martinez, R., Ordonez-Sanchez, S., Lloyd, C., O'doherty, T., Germain, G., Gaurier, B. and Johnstone, C., 2021. A phenomenological study of lab-scale tidal turbine loading under combined irregular wave and shear flow conditions. *Journal of Marine Science and Engineering*, *9*(6), p.593.
[44] P. Mycek, B. Gaurier, G. Germain, G. Pinon, and E. Rivoalen, "Experimental study of the turbulence intensity effects on marine current turbines behaviour. Part I: One single turbine," Renew. Energy, vol. 66, pp. 729–746, Jun. 2014.